ACS APPLIED NANO MATERIALS

www.acsanm.org

Article

Shape-Induced Enhanced Raman Scattering (SIERS) Platforms Modified with Gold Nanorods for Ultradiluted Atrazine Pesticide Detection

Matheus Gomes Ferreira, Anerise de Barros, Flavio Makoto Shimizu, Fernando Aparecido Sigoli, Carlos César Bof Bufon, and Italo Odone Mazali*

Cite This: *ACS Appl. Nano Mater.* 2025, 8, 10287−10296

Read Online

ACCESS | Metrics & More | Article Recommendations | Supporting Information

ABSTRACT: Herein, we explored the shape-induced enhanced Raman scattering (SIERS) effect to detect Atrazine pesticides in different concentrations (1.6×10^{-8}−1.6×10^{-20} mol L^{-1}). For this, the performance of the SIERS effect compared to the conventional Raman signal was evaluated using a silicon substrate with a V-shaped (Si−V) microchannel and a flat silicon substrate (flat Si). Experimental data free of metallic nanostructure show that the SIERS effect increases up to a 7-fold signal for the Atrazine molecule compared to the conventional Raman signal. Combining SIERS and surface-enhanced Raman scattering (SERS) effects (SIERS@SERS) using metallic nanostructures is the key feature used to achieve lower limit detection of the target molecule. The performance of SIERS@SERS was evaluated by using gold nanorods (AuNRs) metallic structure deposited onto Si−V and flat Si for the detection of Atrazine in different concentrations (1.6×10^{-8}−1.6×10^{-20} mol L^{-1}). The geometric design of V-shaped microchannels also enables a "trap" for the molecule confinement and builds up an excellent electromagnetic field distribution by AuNR aggregates. The AuNRs aggregation is also favored by incubating a AuNRs colloidal suspension mixed with Atrazine using different solvents (water and methanol). In this sense, the results reveal that the solvent plays an important role in the signal intensity as well as spectra definition and band identification. The IDMAP statistical projection reveals good data discrimination with a silhouette coefficient of 0.64 for Si−V substrate (1.6×10^{-8}−1.6×10^{-20} mol L^{-1}) against 0.51 for flat Si (1.6×10^{-8}−1.6×10^{-16} mol L^{-1}), indicating that the SIERS@SERS effect provides more sensitivity for the sensor. The Si−V platforms are a robust option for commercial sensors, since they can be reusable with or without plasmonic nanostructures.

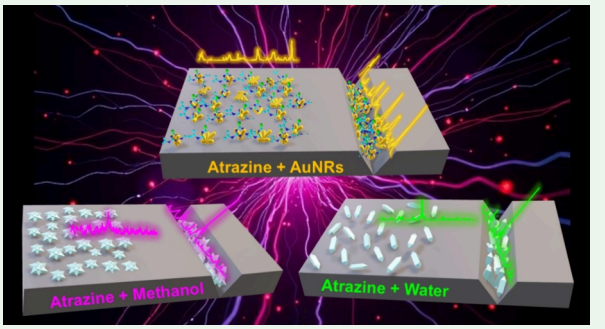

KEYWORDS: *SIERS, SERS, microchannel, atrazine, gold nanorods*

1. INTRODUCTION

Since surface-enhanced Raman scattering (SERS) associated with the Raman technique was reported in the 1970s,[1,2] there is no doubt that SERS is a powerful tool.[3−7] However, the SERS technique presents limitations that hinder its applicability as an analytical tool.[8,9] Panneerselvan et al.[10] reported the main bottlenecks and future directions of the SERS technique, being one of the most difficult in developing easy-to-use and low-cost SERS substrates with high stability and reproducibility. Another factor is the low control of metallic nanoparticle deposition onto substrates, which affects the reproducibility of the SERS substrates.[11−13] In this way, some strategies have been developed to obtain robust SERS substrates based on the reusable nature of these platforms, such as facile removal of metallic nanostructure and further easy decorating.[14,15] For instance, 3D SERS substrates based on the silicon nanowire coated with silver nanoparticles (AgNSph) reached a reusability count of ten times after a simple cleaning step without compromising the Si nanowire structures by removing only the AgNSphs, to detect R6G up to 1×10^{-7} mol L^{-1}.[16] Reusable porous silver nanosheets were developed for organochloride pesticide detection, reaching a 20-fold reusability count.[17] The authors mentioned that the platforms are sensitive to several analytes, regardless of their affinity to a metal surface. The platforms were evaluated using rhodamine B, dichlorodiphenyltrichloromethane, and lindane up to a concentration of 10^{-7} mol L^{-1}. The platforms were reusable 20 times, with SERS activity reproducible. Although these strategies are interesting, they still displayed a higher

Received: December 26, 2024
Revised: April 28, 2025
Accepted: May 1, 2025
Published: May 12, 2025

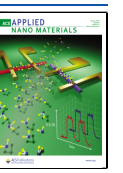

concentration detection in the micromolar range, leading to a limited application as an analytical tool. Therefore, obtaining SERS substrates with more sensitive responses in low-level sample concentrations is still an enormous challenge.

Nowadays, the development of SERS substrates carved cavities in silicon substrates with a metallic thin film of Silver or Gold (Ag or Au), in which the SERS effect is based on the SPR mechanism for noble metal substrates, is growing considerably, mainly for waveguide SERS applications.[18−20] The most significant advantage of a SERS substrate with a cavity is the hot spot region generated by its own cavity, increasing the probability of finding a high molecule concentration under confinement. In this context, our group developed SERS substrates with carved V-shaped microchannels on the Si substrate (Si−V) and modified with gold nanorods (AuNRs) to detect R6G as proof of concept.[21] We verified that Si−V microchannels can enhance the Raman signal by up to 5-fold for R6G, even in the absence of AuNRs. The Si−V platforms modified with AuNRs allowed the detection of attomolar (10^{-18} mol L^{-1}) R6G, and 10^{-10} mol L^{-1} for thiram molecule.[21,22] We called this phenomenon shape-induced enhanced Raman scattering (SIERS), which is associated with electric field intensification caused by constructive interference patterns of light radiation from the V-shaped cavity. The effect induced by the geometric design carved in the silicon substrate was also demonstrated by Mamich et al.,[23] in which 1.0 μm^2 cavities under the wavelength excitation close to the Si cavity width act as a matrix, increasing the Raman scattering efficiency for different analytes embedded inside the cavities. In this case, the authors suggest that partial light localization is strongly generated due to the thin metallic film recovered in these cavities that acts as a waveguide propagation of the excitation light, and as a result, it occurs by increasing the Raman scattering efficiency. In contrast, the SIERS effect is also associated with light confinement, regardless of whether a metallic thin film or metallic nanostructures enhance the Raman signal; i.e., the Raman signal intensification occurs by only cavity geometric design.

One of the main advantages of the Si−V substrates is that they could also be reusable through a cleaning protocol to remove the analyte and metallic nanoparticles, allowing the modification with metallic nanostructures of different morphologies and composition, adjusting the better conditions analysis for specific analytes with lower detection limits being an up-and-coming platform from a commercial point of view. However, understanding how the SIERS effect combined with the SERS effect provides the metallic nanostructures can be improved to scatter Raman signals is still required under several analysis conditions, composition, and target molecules in a lower concentration. Combining the Si−V substrates with metallic nanoparticles can be an excellent alternative to creating efficient SERS substrates with high reproducibility and sensitivity. Different from our previous work,[21,22] in which the analyte (Thiram) was sequentially deposited after the AuNR colloidal suspension was dried onto the Si−V substrate, the present study demonstrates that analyte detection still depends on an optimization process specific to each analyte type. This optimization is crucial to understanding the interfacial interactions between the metallic surface and the analyte in order to enhance the detection performance using this technique. In fact, we continue to demonstrate that the SIERS effect represents a unique active platform that acts as a "trap," promoting the aggregation of both metallic nanostructures and analyte molecules. Based on this, we evaluated how the SIERS effect can contribute to detecting a more complex molecule, such as Atrazine, that has a weak interaction with gold metallic surfaces. For this, different concentrations of Atrazine molecule solutions were evaluated by SIERS@SERS using a Si−V substrate to compare the effect on atrazine pollutant detection in different concentrations against flat Si substrate. In addition, the SIERS and Raman signal free of metallic nanoparticles were evaluated for Atrazine diluted in various solvents, ultrapure water, and methanol. The Raman signal intensity without the plasmonic nanostructure effect was assessed to explore the SIERS effect in atrazine detection, while the influence of the solvent directly impacted the Raman and SIERS spectra profile. The functions of gold nanorods combined with the SIERS effect (SERS@SIERS) were the key features to achieving subattomolar atrazine detection.

2. MATERIALS AND METHODS

2.1. Materials. Hexamethyldisilazane (HMDS), AZ nLOF 2020 photoresist, and AZ 726 MIF developer were purchased from MicroChemicals. The following reagents were purchased from Sigma-Aldrich: 1-Chloro-3-ethylamino-5-isopropylamino-2,4,6-triazine (Atrazine PESTANAL—$C_8H_{14}ClN$, ≥98%), tetrachloroauric (III) acid trihydrated ($HAuCl_4.3H_2O$), hexadecyltrimethylammonium bromide (CTAB ≥ 98%), and potassium hydroxide (KOH, 90%). Sodium Hydroxide (NaOH, P.A.), hydrogen peroxide (H_2O_2, 29%), acetone (C_3H_6O, P.A.), acetone (C_3H_6O, VLSI), isopropyl alcohol (C_3H_7OH, VLSI), and methanol (CH_3OH, P.A.) were purchased from Synth. Isopropyl alcohol (C_3H_7OH, P.A.) was purchased from Synth. The Millipore Synergy UV obtained ultrapure water with 18.2 MΩ.

2.2. Characterization of AuNRs and Si−V Substrates. UV−vis spectroscopy was performed to determine the extinction spectra of the AuNRs colloidal suspension by using a Cary 50 spectrophotometer. Transmission electron microscopy (TEM) was also performed to characterize the AuNRs by drop drying 10 μL of the concentrated suspension in a holey carbon-coated Cu grid using a Libra Zeiss 120 transmission electron microscope. The size distribution of the AuNRs was obtained by using the ImageJ software by counting 500 particles. The AuNRs synthesis is described in the Supporting Information. The Si−V substrates were fabricated using the procedure described by Bär et al.,[21] and during the corrosion processes, confocal images were obtained using a 3D laser scanning confocal microscope - VKX200 (Keyence), Wavelength—408 nm (violet) to evaluate the depth and aperture length of the V-shaped microchannels. Scanning electron microscopy (SEM) was also performed after the microfabrication process to characterize the quality of the surface of the substrates and after sample deposition, using a scanning electron microscope model FEI Quanta 250 FEG (FEI Co., USA), with voltage acceleration of 20 kV in a tungsten filament.

2.3. Si−V and Flat Si Substrate Preparation for Raman Analysis. The Raman and SIERS spectra for the atrazine target molecule were collected for Si−V and flat Si substrates without AuNRs. For this, a stock solution of 1.6×10^{-2} mol L^{-1} in methanol solvent, and subsequent dilutions were prepared for 1.6×10^{-4}−1.6×10^{-6} mol L^{-1} in ultrapure water, and methanol. (i) Raman characterization: An aliquot of 10.00 ± 0.12 μL of atrazine (1.6×10^{-4}−1.6×10^{-6} mol L^{-1}) solution in different solvents (ultrapure water and methanol) was dropped individually onto Si−V and flat Si substrates and dried at ambient temperature (~25 °C). This process was repeated four times, entirely 40 μL dropped. It is important to mention that the Si−V and flat Si substrates are supported in a glass slide with a 5° inclination to favor their flows into the Si−V channels through capillarity, and the substrates were turned 180° for each aliquot dropped. (ii) SIERS@SERS characterization: Si−V and flat Si substrates for SIERS@SERS spectra acquisition were prepared from

https://doi.org/10.1021/acsanm.4c07289
ACS Appl. Nano Mater. 2025, 8, 10287−10296

optimization of AuNRs incubation with atrazine target molecules at a 1.6×10^{-8}–1.6×10^{-20} mol L^{-1} range of concentrations. Briefly, 10.00 ± 0.12 μL of ultrapure water, 10.00 ± 0.12 μL of AuNRs colloidal suspension, and 40 μL of Atrazine solution were kindly mixed and incubated for 30 min. A detailed description of the Atrazine solution proportion in methanol and ultrapure water for each concentration is included in Table S1. After the incubation period, the incubation solution was dropped onto the Si−V and flat Si substrates every 10 μL and dried at environment temperature (~25 °C). The substrates (Si−V and flat Si) were supported in a glass slide with a 5° inclination to favor their flow into the Si−V channels through capillarity, and turned 180° for each aliquot dropped. This process was repeated six times, with a volume of 60 μL dropped, corresponding to the entire solution incubated.

2.4. Silicon Substrates Clean Protocol (Si−V and Si Flat). A cleaning protocol was established and optimized, ensuring the complete removal of AuNRs-atrazine for further Si−V and flat Si reuse. The steps are described as (i) precleaning using a damp cotton swab in acetone (C_3H_6O, P.A.) followed by ultrapure water washing; (ii) the same procedure described in (i) was performed by using isopropyl alcohol (C_3H7OH, P.A.); (iii) this step is only performed for Si−V and flat Si-containing AuNRs, the substrates are immersed in an aqua-regia (3:1 v/v HCl:HNO_3) solution for 10 min; (iv) in the sequence, Si−V and flat Si are immersed in piranha solution 4:1 v/v H_2SO_4:H_2O_2 for 30 min, then washed in abundance with ultrapure water; (v) the Si−V and flat Si are immersed in a solution 1:1:3 v/v/v NH_4OH:H_2O_2:H_2O and heated ~85 °C for 20 min, then washed with ultrapure water; (vi) the same procedure described in (v) is performed by using a solution 1:1:4 v/v/v HCl:H_2O_2:H_2O, heated ~85 °C for 20 min, followed washing with ultrapure water. Finally, the Si−V and flat Si were dried by using a flow of N_2. Although the reusability of Si−V substrates has not been explored in this study, they were used many times after a clean protocol.

2.5. Raman Analysis. Raman and SIERS@SERS spectra were collected using a HORIBA Jobin Yvon T64000 Raman spectrometer coupled with an Olympus BX41 microscope and a charge-coupled device detector using a laser of 633 nm from a He−Ne laser (Research Electro-Optics) as incident radiation. The 663 nm laser was chosen based on De Barros et al.,[24] whose BEM simulations show that the gold nanorods aggregation leads to the shifted excitation band at 748 nm to near 633 nm. The Raman spectra for the Atrazine and CTAB powder were collected using a 50xLWD objective lens, with one accumulation in the exposure time of 20 s, in 600 grooves/m^2 grade. The SIERS and Raman spectra were collected without AuNRs for Si−V and flat Si substrates. The spectra on the flat Si were collected using a 100xLWD objective lens, with one accumulation in the exposure time of 20 s in the 600 grooves/mm^2 grade in a mapping mode. For the Si−V substrates, the spectra were collected using a 50× LWD objective lens with one accumulation and exposure time of 20 s in a mapping mode, grade of 600 grooves/mm^2. For the Si−V and flat Si with AuNRs deposited, the SIERS@SERS were collected using a 10× objective lens, with one accumulation in the exposure time of 20 s, in the 600 grooves/mm^2 grade for mapping mode. The calibration of the spectrometer was performed using a crystalline band of the Si substrate at 520.7 cm^{-1}. To collect the spectra on mapping mode inside the V-shaped microchannels, the grid with the region of interest to collect the spectra was placed in the middle region of the microchannel opening, which has dimensions of roughly 6.5 μm, as depicted in Figure S1. The area of the beam calculated by the use of the 10x objective lens, which has an aperture value of 0.25, was 1.3 μm^2. The SIERS@SERS and SERS performance of the substrates (Si−V and flat Si) were evaluated using solutions of Atrazine as the target molecule.

2.6. Multivariate Analysis. Raman spectra were analyzed by using unsupervised and supervised multivariate methods. First, a pretreatment is performed in all data sets by correcting scattering effects, commonly observed in spectroscopic assays, using an extended multiplicative scattering correction algorithm (EMSC), with a sixth-order polynomial. For the unsupervised clustering analysis, the Interactive Document Map (IDMAP) projection technique[25] was applied to normalized data sets in the selected region, 580 and 1650 cm^{-1}, to avoid silicon vibrational band response. A supervised multilabel classification model was performed using the Explainable Matrix (ExMatrix) algorithm,[26] a visualization tool to explain decision tree (DT) classification results through logical rules that provide predictability through the multidimensional calibration space (MCS) technique.[27] All data were separated into training and test data sets in a ratio of 70/30. 5 k-fold cross-validation was applied to avoid biased or overfitting problems, and all analyses were performed using Python Algorithms.

3. RESULTS AND DISCUSSION

Effective AuNRs synthesis was achieved and characterized by UV−vis spectroscopy (Figure S2a) displaying the plasmon bands at 514 and 746 nm, corresponding to the transverse surface plasmon resonance and longitudinal surface plasmon resonance (TSPR and LSPR),[24,28] respectively. The narrowness of the band at 746 nm can indicate the low amount of other morphologies and a good size distribution due to the synthesis protocol performance. Corroborating with this result, TEM micrographs (Figure S2c−f) indicated an excellent homogeneity for the nanorods, and the histogram (Figure S2b) exhibited a narrow size distribution with a size of 51 ± 4 and 12.5 ± 1.8 nm for length and width, respectively. The high homogeneity obtained for AuNRs is essential to further evaluate their functions in SERS and SIERS@SERS active platforms by target molecule interaction. Moreover, the AuNRs have the main advantage of their optical plasmonic advantages, such as their anisotropic structure and characteristic plasmon resonance in a longitudinal and transverse mode, which can provide more efficient signal intensification depending on the region in which the target molecule is adsorbed. Si−V microchannels were characterized by SEM micrographs, as can be seen in Figure S1g−i. Herein, Si−V substrates previously fabricated by Bär et al.,[21] and new ones fabricated, were used and characterized. Figure S1a−f reveals that the microfabrication process of new Si−V substrates is very reproducible, whose micrograph in Figure S1g corresponds to the Si−V substrates fabricated by Bär et al.,[21] and Figure S1h,i obtained in this work.

The Raman analysis for neat CTAB (capping surfactant used for AuNRs) and neat Atrazine powders was acquired to identify the best reference band for Atrazine monitoring, which does not overlap any CTAB band. Figure 1 shows the prominent Raman bands at 437, 726, 738, 760, 898, 919, 945, 1020, 1057, 1086, 1106, 1255, 1362, 1408, 1432, and 1448 cm^{-1} for CTAB (red line), and 417, 646, 684, 838, 922, 963,

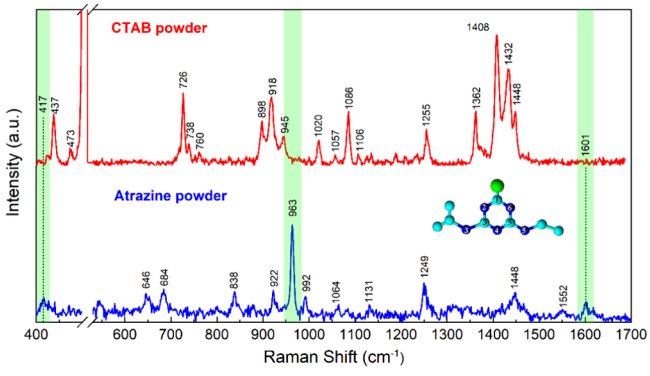

Figure 1. Raman spectra for CTAB powder (red line) and atrazine powder (blue line).

https://doi.org/10.1021/acsanm.4c07289
ACS Appl. Nano Mater. 2025, 8, 10287−10296

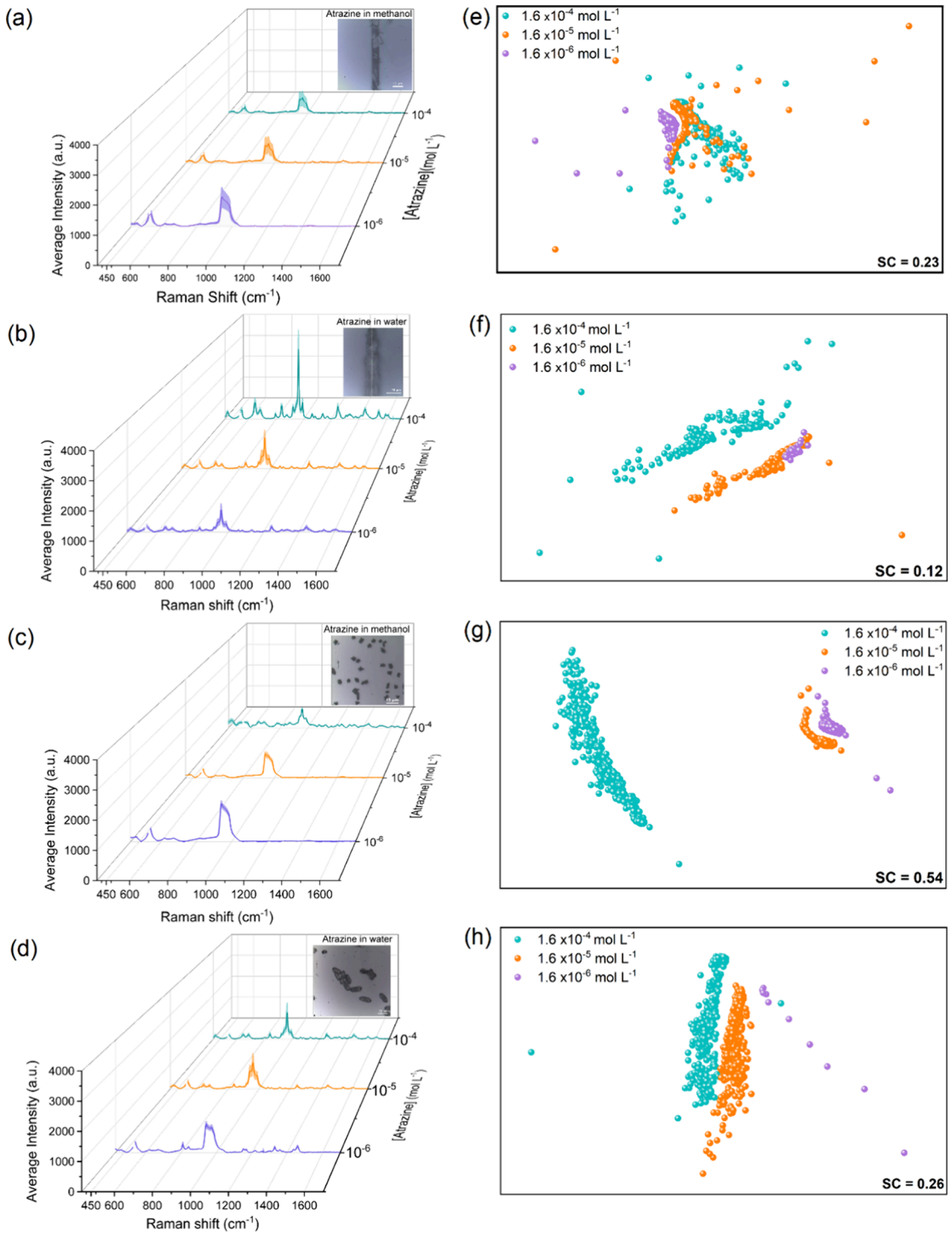

Figure 2. Atrazine solution in the range of 1.6×10^{-4}–1.6×10^{-6} mol L^{-1} characterized by SIERS spectra in methanol solvent in (a) and water solvent in (b), both in Si–V substrates. Raman spectra for Atrazine solution in the range of 1.6×10^{-4}–1.6×10^{-6} mol L^{-1} characterized in methanol solvent in (c) and water solvent in (d) for flat Si substrates. The insets correspond to the Raman optical images for the Si–V and flat Si for the exact region of SIERS spectra collected. (e–h) correspond to the IDMAP statistic projections for each analysis condition displayed in (a–d).

992, 1064, 1249, 1448, 1552, and 1601 cm^{-1} for Atrazine (blue line). Note that the Atrazine bands are very close to the CTAB bands, whose most intense band of Atrazine appears at 963 cm^{-1}, while a weak band at 1601 cm^{-1} for Atrazine appears in a region absent of CTAB bands. In this sense, we previously chose the bands at 417, 963, and 1601 cm^{-1} as references for Raman, SERS, and SIERS@SERS characterization. A comparison and assignments of CTAB and atrazine bands can be seen in Table S2.

In order to prove how the SIERS effect can be more sensitive than traditional Raman analysis, we evaluated the Atrazine spectra on the Si–V and flat Si substrates free of metallic nanostructures (Figure 2a–d) in the concentration range of 1.6×10^{-4}–1.6×10^{-6} mol L^{-1}. In addition, we

https://doi.org/10.1021/acsanm.4c07289
ACS Appl. Nano Mater. 2025, 8, 10287–10296

Scheme 1. Schematic Representation of AuNRs and Atrazine Sample Preparation by the Incubation Process Followed by AuNRs-Atrazine Deposition onto Si−V Substrates

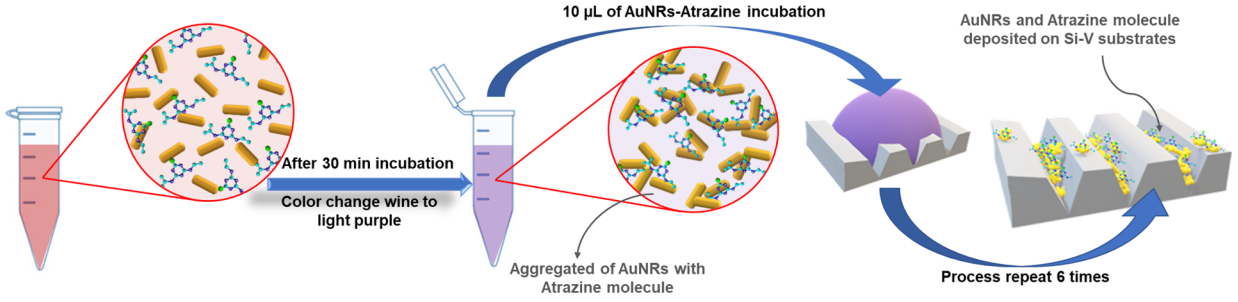

evaluated the effects in the SIERS and Raman spectra using different solvents for Atrazine dilution (methanol and water) since Atrazine is better diluted in methanol than in water. For this, a stock solution of 1.6×10^{-2} mol L^{-1} in methanol and successive dilutions were prepared in methanol and ultrapure water for SIERS and Raman spectra comparison. It is essential to be clear that the SIERS spectrum is associated with the Si−V microchannels, while the Raman spectrum corresponds to the flat Si substrate, i.e., in both cases, the analyses were performed free of metallic nanostructures.

Figure 2a shows that Atrazine diluted in methanol displayed lower signal intensity SIERS spectra. Consequently, the bands are poorly identified, while the SIERS spectra for Atrazine diluted in ultrapure water (Figure 2b) have an improved SIERS signal and better spectral profile definition for all concentrations (1.6×10^{-4}−1.6×10^{-6} mol L^{-1}). A similar behavior is observed for the Raman spectra in Figure 2c,d, whose highest intensity spectra are observed in Figure 2d for Atrazine in ultrapure water. These results indicate that the solvent influences the signal of Raman spectra independently of the substrates analyzed. More specifically, we observed from the optical images shown in the inset of Figure 2a−d that the solvent influences the way Atrazine crystal aggregates, which can be associated with the drying speed ratio.[29,30] Despite these different crystal morphologies and aggregations already reported in the literature for other molecules,[31,32] there are no reports on how crystallinity actually impacts the Raman spectrum of Atrazine. However, further studies are needed to better understand the role of the solvent in the crystallization process of Atrazine and its influence on the quality of the Raman spectra. Regardless, for the SIERS spectra in Figure 2a,b, the slower evaporation rate for the ultrapure water favored more Atrazine molecule aggregates inside the Si−V microchannels. In addition, the SIERS effect contributes to the signal increase due to the electric field intensification in the edges and vicinity of V-shaped microchannels, as previously shown in our published work.[21] A set of SIERS and Raman mapping can be seen in Figures S3a−c and S4a−c in the Supporting Information.

Comparing the signal intensity of SIERS and conventional Raman, both free of metallic nanostructure (Figure 2b,d), an approximately 3-fold increase for the SIERS spectra is observed concerning conventional Raman spectra for Atrazine 1.6×10^{-4} mol L^{-1} diluted in ultrapure water. Additionally, compared to the Raman spectrum of Atrazine in neat powder, the SIERS signal increased 2−7-fold for the 1.6×10^{-6} and 1.6×10^{-4} mol L^{-1} concentrations, indicating an excellent performance of SIERS as platforms free of metallic nanostructure and a new alternative of analysis with a small sample amount. It is essential to mention that the enhancement signal provided by SIERS has already been reported by Bär et al.,[21] whose finite-element simulation results show that the maximum enhancement of the scattered electric field can be verified on the V-shaped microchannel edges and their vicinity. Specifically, the electric field enhancement could be reached 50 times for the Si−V microchannel compared with the flat Si substrate. Experimental results show that the signal intensity for the Si band at 520 cm^{-1} can vary depending on the Si−V microchannel region monitored, with an increase of 2−7-fold. As a result, SIERS is very promising for detecting ultradiluted solutions.

Figure 2e−h corresponds to the IDMAP projections for each analysis condition displayed in Figure 2a−d, respectively. Although the silhouette coefficients (SC) are more remarkable for the flat Si (0.54 and 0.26) than Si−V substrates (0.23 and 0.12), it is observed that the SIERS spectra (Figure 2b) displayed better quality in band definitions and a significantly higher intensity than the flat Si. In this sense, obtaining spectra of greater signal intensity can be essential for achieving lower concentration detection. In addition, the multidimensional calibration space using the ExMatrix algorithm was performed for different solvent atrazine conditions, as can be seen in Figure S5a−d. The classification of atrazine concentrations was established inside Si−V and flat Si substrates from 1.6×10^{-7} to 1.6×10^{-6} mol L^{-1} in the frequency range of 580−1650 cm^{-1}, and both analyses needed three logical rules and two features to classify the three concentrations. Note that the atrazine concentrations of 1.6×10^{-5} and 1.6×10^{-6} mol L^{-1} are better distinguished for feature 977 cm^{-1} (Figure S5a,b,d) independently of the solvent used, corroborating with our previous band selection in Figure 1. The feature importance at 940 cm^{-1}, seen in Figure S5a,c,d, can also be associated with the band at 977 cm^{-1}, whose band position could be shifted or broadened.

To verify the SERS and SIERS@SERS performance for the flat Si and Si−V substrates, we optimized an incubation process of AuNRs and Atrazine in concentrations of 1.6×10^{-8}−1.6×10^{-20} mol L^{-1}. Scheme 1 illustrates the sequence preparation of AuNRs and Atrazine deposited on the Si−V substrate; the same process is followed for flat Si substrates. More details of the incubation process for the AuNRs and Atrazine ratios can be seen in Table S1 in the Supporting Information. Figure 3a−c illustrates the SEM micrographs of Si−V modified with AuNRs:Atrazine incubation. It is possible to observe that the sample of AuNRs:Atrazine incubated is predominantly deposited inside the Si−V substrate. However, due to the presence of methanol in the AuNRs:Atrazine solution incubated, the solvent evaporation rate is increased,

https://doi.org/10.1021/acsanm.4c07289
ACS Appl. Nano Mater. 2025, 8, 10287−10296

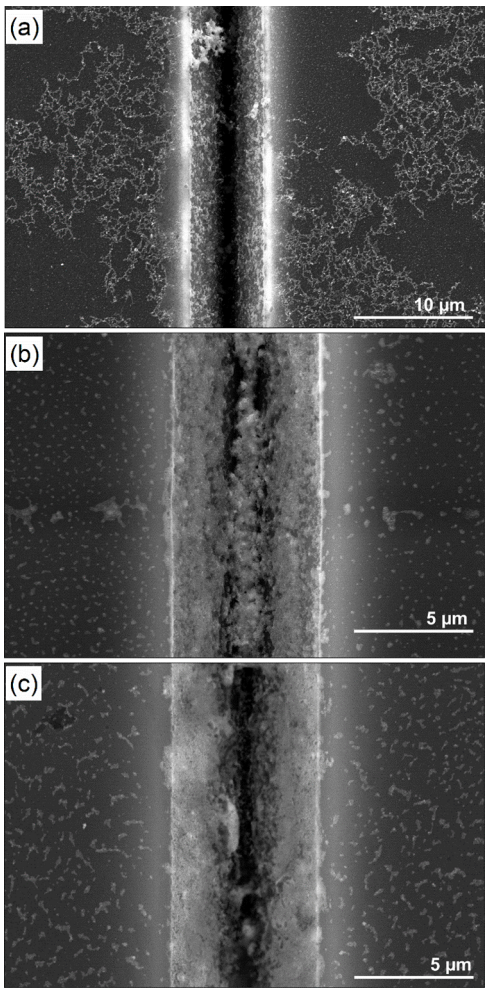

Figure 3. SEM micrographies of Si−V with AuNRs-atrazine deposited by the drop-casting method, using 60 μL of AuNRs-atrazine incubation solution. (a) In magnification of 5000× and (b,c) in magnifications of 10,000×.

and consequently, the AuNRs-atrazine is also deposited on the top of Si−V. This condition for Atrazine ratios diluted in water or methanol mixed with a fixed volume of AuNRs suspension was essential to improve the SERS and SIERS@SERS performance and reach lower concentrations of detection. In addition, the nonfunctionalized substrate was also a determining factor in facilitating the cleaning protocol and making the substrate reusable. Therefore, we can say that the AuNRs deposition is governed only by low-magnitude physisorption, such as van der Waals interactions.

Figure 4a−c shows the average SIERS@SERS and SERS spectra collected in different regions of Si−V and flat Si substrates. The average spectra for each concentration correspond to the set of two hundred spectra that are inserted in the Supporting Information (Figures S6a−f and S7a−f). Observed in Figure 4a,b for the SIERS@SERS spectra, the prominent bands for Atrazine at 417 and 963 cm^{-1} chosen initially are not significantly visible. However, the band at 1601 cm^{-1} appears with a shift at 1617 cm^{-1}, with a higher intensity. Specifically, this band is assigned to the combination of deformations in the plane of the ring and δC3−N3−H modes for the Atrazine molecule, whose spectral changes for atrazine molecules are mainly observed in this region due to the adsorption position of Atrazine molecules on the metallic surface structures as described by Costa et al.[33] Therefore, the band at 1617 cm^{-1} was taken as a reference for the SERS and SIERS@SERS spectra in Figure 4a,b. From the band at 1617 cm^{-1}, we clearly observed that the SIERS@SERS spectra have a 5-fold higher intensity than the SERS spectra for the Atrazine concentration of 1.6×10^{-8} mol L^{-1}. The high intensity observed for higher concentrations allows lower concentrations to be detected, and herein, we achieve the detection until 1.6×10^{-20} mol L^{-1}. According to our results, SIERS@SERS mapping indicates the presence of Atrazine in 10 spectra out of a total of 225 collected, which was identified by the band at 1617 cm^{-1} with an average intensity of 578.6 counts. The spectra were found in 3 microchannels out of a total of 26 carved in the Si substrate. Specifically, these microchannels are identified by letters from A to Z, and we saw 1, 7, and 2 SIERS@SERS spectra in the microchannels A, B, and C, respectively. Despite the probability of picking up one or more being low, it does exist, and to support this issue, we modeled throughout the *distribution of Poisson* the probability of picking up more than a specific number of molecules in an aliquot solution, as well as their cumulative probability. A detailed discussion about the Poisson distribution and all values calculated are inserted in Table S3 in the Supporting Information.

Specifically, the model uses the Poisson distribution, which is suitable for rare events or discrete counts in small volumes. To a concentration of 1.6×10^{-20} mol L^{-1}, we have an average number of molecules of 9.57 for each solution, i.e., atrazine-methanol and Atrazine-ultrapure water. The Poisson distribution indicates that it is possible to have up to 38% more molecules in solution. On the other hand, to prepare the incubation AuNRs:Atrazine, we take smaller aliquots, and the Poisson distribution indicates that it is possible to pick up 11.7% more molecules in an aliquot of 13 μL for Atrazine diluted in methanol, and 22.8% more molecules in an aliquot of 27 μL for Atrazine diluted in water. The cumulative probability indicates that in an aliquot of 13 μL, there is an 88.3% probability of having zero molecules in this volume, 99.1% probability of having one or fewer molecules, 99.98 two or fewer molecules, and 99.998% probability of having three or fewer molecules. To an aliquot of 27 μL, there is a 77.2% probability of having zero molecules in this volume, a 97.1% probability of having one or fewer molecules, a 99.68 two or fewer molecules, and a 99.90% probability of having three or fewer molecules. These results are consistent with the SIERS spectra obtained on the Si−V substrates, indicating that, although the likelihood is low, there remains a probability of collecting a greater number of molecules within a small volume aliquot. This is particularly relevant considering that the stock solution contained approximately 9.57 molecules (for all solutions prepared in methanol and water).

Multivariate projection techniques and unsupervised/supervised methods were applied to better visualize and compare the SIERS@SERS and SERS data sets in Figure 4a,b. As shown in Figure 4c,d, it was corrected using the MSC algorithm applied in IDMAP projection to improve the effects of the light commonly present in Raman experiments. Figure 4c,d shows that an excellent silhouette coefficient (SC) was obtained, 0.64 and 0.51, for the AuNRs-atrazine detection inside Si−V and flat Si−V substrates, respectively. The SC values above 0.5 indicate that significant discrimination was achieved, and the clusters are identified. Although both conditions had SC above 0.5, it is seen that the Si−V substrate

https://doi.org/10.1021/acsanm.4c07289
ACS Appl. Nano Mater. 2025, 8, 10287−10296

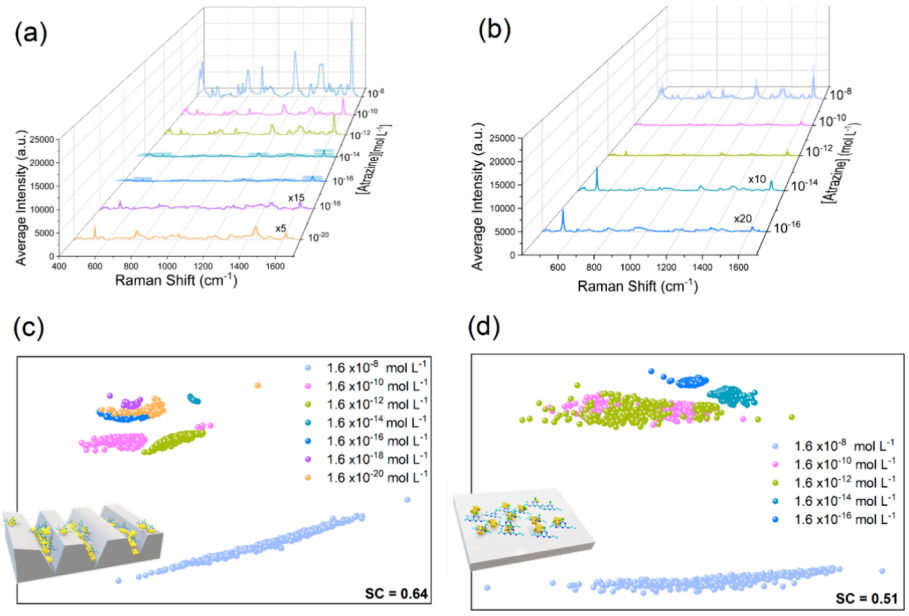

Figure 4. (a) Average SIERS@SERS spectra of AuNRs:Atrazine incubation deposited inside Si−V microchannels; (b) average SERS spectra of AuNRs:Atrazine deposited onto flat Si substrate. IDMAP plot for Raman data set in (c) corresponds to the SIERS@SERS data set of AuNRs:Atrazine incubation deposited inside of Si−V; (d) corresponds to the SERS data set of AuNRs:Atrazine incubation deposited onto flat Si substrate.

can form clusters formed better than a flat Si substrate for ultradiluted concentrations (1.6×10^{-10}–1.6×10^{-20} mol L^{-1}), given a higher SC. Moreover, the intensity of the Si−V substrate is 5-fold higher than that of the flat Si substrate, which allowed for the detection of subattomolar (1.6×10^{-20} mol L^{-1}) concentration for Atrazine. It is important to mention atrazine detection at lower concentrations regardless of the nanostructure composition, i.e., if they have a gold or silver composition. For instance, the atrazine detection up to 10^{-12} mol L^{-1}[34,35] was only achieved for the substrate using silver nanoparticles (AgNPs),[34,35] due to the amine group interaction with the AgNP surface. In contrast, gold nanoparticles (AuNPs) deposited on a silicon wafer substrate had been reported as having a lower atrazine detection of 10^{-5} mol L^{-1}.[36] Thus, by combining the SIERS effect and plasmonic gold nanoparticles, i.e., the SIERS@SERS effect, it was possible to achieve the lowest concentration detection for the atrazine molecule. Specifically, the Raman signal is enhanced by constructive interferences inside Si−V microchannels, called the SIERS effect, whose simulated results showed that the locations with the maximum enhancement of scattered electric field could be noticed on the V-shaped microchannel edges and their vicinity, providing more interference patterns from the scattered electric field propagation. As a result, a Raman signal enhancement will occur in constructive interference due to the electric field intensification that can reach up to 50 times the intensity of the incident radiation on the walls and edges of V-shaped microchannels.[21] Moreover, the use of SIERS platforms (Si−V microchannels) combined with the SERS effect, using AuNRs, allows for reaching lower concentrations, such as in a single molecule regime detection, that are unobserved by only the SERS effect (flat Si with AuNRs). The SIERS platforms have the advantage of their reuse, no surface functionalization required to adhere metal nanostructures, and their use without any metallic nanostructure, which still allows submicromolar detection. On the other hand, the SIERS effects provided by V-shaped, combined with optimized AuNRs and target molecule incubation, lead to lower concentration detection. The calculation of the analytical enhancement factor (AEF) for both conditions, SERS and SIERS@SERS, becomes a challenge, as many factors that make quantification unfeasible, such as the orientation of the molecule adsorbed on the surface of the metallic nanostructures, seem to play a role in the enhancement process. This can be seen by the preferential enhancement of bands that were not the most intense in the bulk phase, like the bands in 417 and 1601 cm^{-1}, which were the latter ones that shifted to higher wave numbers. Therefore, the conventional AEF parameter is unsuitable for characterizing the enhancement provided by the Si−V substrate (SIERS effect) in combination with SERS in the presence of the AuNRs.

The atrazine detection assay was further calibrated with multidimensional calibration space using the ExMatrix algorithm. The classification of atrazine concentrations was established inside the Si−V microchannel (classes 1.6×10^{-8}–1.6×10^{-20} mol L^{-1}) and the flat Si substrate (classes 1.6×10^{-8}–1.6×10^{-16} mol L^{-1}) with an accuracy of 99% for two models. More than 300 spectra were collected for each concentration in the 580–1650 cm^{-1} frequency range, yielding 790 features. Figure 5a displays the ExMatrix representation for the atrazine detection inside the Si−V microchannel, in which only seven logical rules and six features were required to classify the seven concentrations. It is worth mentioning that five features (913, 940, 977, 1172, and 1378 cm^{-1}) have the same importance (17%), but the last, 1298 cm^{-1}, has 15%. The concentrated atrazine solutions, 1.6×10^{-8} and 1.6×10^{-10} mol L^{-1}, can be distinguished from others in the second (940 cm^{-1}) and first (1172 cm^{-1}), respectively. The fourth column (913 cm^{-1}) explains the difference between 1.6×10^{-12} and 1.6×10^{-14}, 1.6×10^{-16}, and 1.6×10^{-20} mol L^{-1}. The fifth column (1378 cm^{-1}) differentiates 1.6×10^{-14} mol L^{-1} from 1.6×10^{-16}, and 1.6×10^{-20} mol L^{-1}. The third and sixth columns discriminate the diluted solutions (1.6×10^{-18} and 1.6×10^{-20} mol L^{-1}) due to the SIERS@SERS effect. As

https://doi.org/10.1021/acsanm.4c07289
ACS Appl. Nano Mater. 2025, 8, 10287−10296

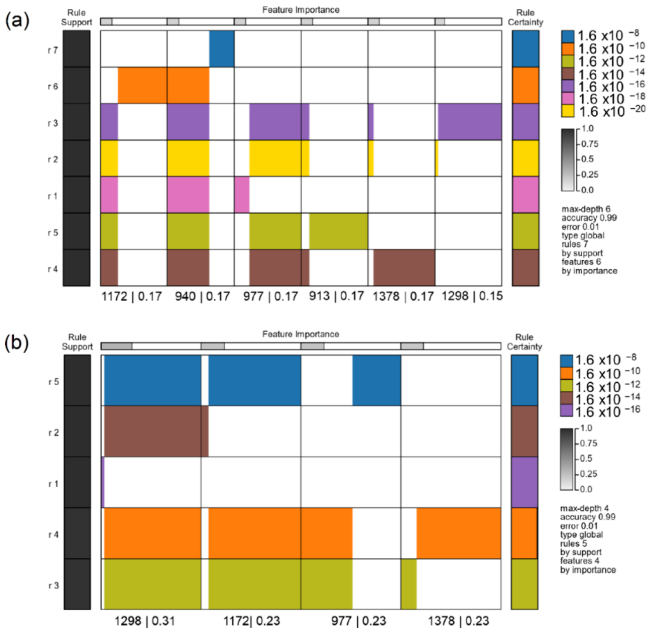

Figure 5. (a) ExMatrix representation using the DT with seven logic rules and six features for the SIERS@SERS data set spectra, Si−V substrate modified with AuNRs:Atrazine incubation in different concentrations. (b) ExMatrix representation using the DT with five logic rules and four features for the SERS data set spectra, flat Si substrates modified with AuNRs-atrazine incubation in different concentrations.

expected, the flat Si with AuNRs-atrazine incubation allowed the detection of a more concentrated atrazine solution, up to 1.6×10^{-16} mol L^{-1}, since the amplification is limited to the SERS effect only. Figure 5b shows the ExMatrix representation for the flat Si surface, which required five logical rules and four features to classify the five atrazine concentrations. The most important feature (1298 cm^{-1}, 31%) explains the difference between the 1.6×10^{-16} mol L^{-1} diluted solution and the more concentrated ones. The remaining columns present the same importance (23%) and allow discrimination of the 1.6×10^{-14} from 1.6×10^{-8}, 1.6×10^{-10}, and 1.6×10^{-12} mol L^{-1}, the 1.6×10^{-8} from 1.6×10^{-10} and 1.6×10^{-12} mol L^{-1}, and 1.6×10^{-10} from 1.6×10^{-12} mol L^{-1}, respectively.

4. CONCLUSIONS

We demonstrated that the SIERS effect can be more sensitive than the traditional Raman spectrum, in which unobserved bands in Atrazine neat powder for conventional Raman spectra were more evident in SIERS spectra. Besides this, the SIERS spectra for Atrazine solution displayed an increasing intensity signal of 2−7-fold compared to the traditional Raman spectra for neat Atrazine powder. This result shows the excellent performance obtained for Si−V platforms due to the SIERS effect, whose substrate can be an alternative for analysis with a small sample volume, free of metallic nanostructures, and reach up to a micromolar range detection. In addition, we observed that the solvent has an important role in the signal intensity and spectra profile, decreasing signal/noise in the spectra and better highlighting the bands of the target molecule. More specifically, the Atrazine diluted in water solvent provided higher SIERS and Raman signal intensity than the one prepared in methanol, with a better spectra profile definition. The ExMatrix classification results show that the lower concentrations (1.6×10^{-5} and 1.6×10^{-6} mol L^{-1}) for SIERS and Raman spectra are better discriminated by the band at 977 cm^{-1}, regardless of the solvent. On the other hand, the synergy of the SIERS effect and SERS effect provided by plasmonic nanostructures (SIERS@SERS) increases the Raman signal intensity, which improves the sensitivity of the platforms, allowing the subattomolar (1.6×10^{-20} mol L^{-1}) Atrazine detection. The detection achieved for Atrazine in this work is the lowest concentration detected and reported by AuNRs. The IDMAP results displayed an SC of 0.51 for the flat Si substrate in a range of 1.6×10^{-8}−10^{-16} mol L^{-1} against 0.64 for Si−V substrate in 1.6×10^{-8}−1.6×10^{-20} mol L^{-1}, indicating high sensitivity for Si−V substrate in the detection of ultradiluted sample. Although the probability of picking up one or more is low, it does exist, and the Poisson distribution indicates that it is possible to have up to 38% more molecules in a 1.6×10^{-20} mol L^{-1} Atrazine solution. On the other hand, the cumulative probability indicates that in an aliquot of 13 μL, there is an 88.3% probability of having zero molecules in this volume, 99.1% probability of having one or fewer molecules, 99.98 two or fewer molecules, and 99.998% probability of having three or fewer molecules. To an aliquot of 27 μL, there is a 77.2% probability of having zero molecules in this volume, a 97.1% probability of having one or fewer molecules, a 99.68 two or fewer molecules, and a 99.90% probability of having three or fewer molecules. This result corroborates SIERS@SERS mapping, which indicates the presence of Atrazine in 10 spectra out of a total of 225 collected, which was identified by the band at 1617 cm^{-1} with an average intensity of 578.6 counts. The spectra were collected in 3 microchannels out of a total of 26 carved in the Si substrate. Additionally, the Si−V substrate offers reusability, a significant advantage for applications with and without plasmonic nanostructures. Moreover, combining plasmonic nanostructures with the SIERS effect enhances sensitivity, enabling lower detection limits and opening a new future for the SERS tool, as well as an analytical strategy and commercial application.

■ ASSOCIATED CONTENT

Supporting Information

The Supporting Information is available free of charge at https://pubs.acs.org/doi/10.1021/acsanm.4c07289.

Synthesis AuNRs procedure, Si−V litograph process, AuNRs incubation with atrazine details. Complementary characterization of UV, TEM, confocal microscopy, ExMatrix, SIERS/SERS, and Raman spectra (PDF)

■ AUTHOR INFORMATION

Corresponding Author

Italo Odone Mazali − *Instituto de Química (IQ), Laboratório de Materiais Funcionais, Universidade Estadual de Campinas, UNICAMP, 13083-970 Campinas, São Paulo, Brazil*; orcid.org/0000-0001-5698-5273; Email: mazali@unicamp.br

Authors

Matheus Gomes Ferreira − *Instituto de Química (IQ), Laboratório de Materiais Funcionais, Universidade Estadual de Campinas, UNICAMP, 13083-970 Campinas, São Paulo, Brazil*

Anerise de Barros − *Instituto de Química (IQ), Laboratório de Materiais Funcionais, Universidade Estadual de*

https://doi.org/10.1021/acsanm.4c07289
ACS Appl. Nano Mater. 2025, 8, 10287−10296

Campinas, UNICAMP, 13083-970 Campinas, São Paulo, Brazil; orcid.org/0000-0002-1616-2368

Flavio Makoto Shimizu − *Instituto de Física Gleb Wataghin (IFGW), Departamento de Física Aplicada, Universidade Estadual de Campinas, UNICAMP, 13083-859 Campinas, São Paulo, Brazil;* orcid.org/0000-0002-4833-9893

Fernando Aparecido Sigoli − *Instituto de Química (IQ), Laboratório de Materiais Funcionais, Universidade Estadual de Campinas, UNICAMP, 13083-970 Campinas, São Paulo, Brazil;* orcid.org/0000-0003-1285-6765

Carlos César Bof Bufon − *Instituto de Geocîências and Cîências Exatas (IGCE), Departamento de Física, Universidade Estadual Paulista "Julio de Mesquita Filho", UNESP, 13506-900 Rio Claro, São Paulo, Brazil*

Complete contact information is available at: https://pubs.acs.org/10.1021/acsanm.4c07289

Funding

The Article Processing Charge for the publication of this research was funded by the Coordenacao de Aperfeicoamento de Pessoal de Nivel Superior (CAPES), Brazil (ROR identifier: 00x0ma614).

Notes

The authors declare no competing financial interest.

■ ACKNOWLEDGMENTS

The authors gratefully acknowledge the financial support provided by CNPq (310131/2020-0, 310745/2022-5, 405087/2021-7, 465452/2014-0) FAPESP (2022/02893-1, 2014/50906-9), and CAPES (Finance Code 001) financed MSc. Student Matheus G. Ferreira. Contributions from the National Nanotechnology Laboratory (LNNano-CNPEM, Brazil) and Multiused Laboratory of Advanced Optical Spectroscopy (LMEOA/IQ-UNICAMP) analysis are also gratefully acknowledged. These contribute to the National Institute of Science and Technology in Complex Functional Materials (CNPq-MCT/FAPESP).

■ REFERENCES

(1) Fleischmann, M.; Hendra, P. J.; McQuillan, A. J. Raman Spectra of Pyridine Adsorbed At a Silver Electrode. *Chem. Phys. Lett.* **1974**, *6* (2), 163−166.

(2) Le Ru, E. C.; Auguié, B. Enhancement Factors: A Central Concept during 50 Years of Surface-Enhanced Raman Spectroscopy. *ACS Nano* **2024**, *18* (14), 9773−9783.

(3) Ma, H.; Pan, S. Q.; Wang, W. L.; Yue, X.; Xi, X. H.; Yan, S.; Wu, D. Y.; Wang, X.; Liu, G.; Ren, B. Surface-Enhanced Raman Spectroscopy: Current Understanding, Challenges, and Opportunities. *ACS Nano* **2024**, *18* (22), 14000−14019.

(4) Itoh, T.; Procházka, M.; Dong, Z. C.; Ji, W.; Yamamoto, Y. S.; Zhang, Y.; Ozaki, Y. Toward a New Era of SERS and TERS at the Nanometer Scale: From Fundamentals to Innovative Applications. *Chem. Rev.* **2023**, *123* (4), 1552−1634.

(5) Liu, X.; Guo, J.; Li, Y.; Wang, B.; Yang, S.; Chen, W.; Wu, X.; Guo, J.; Ma, X. SERS Substrate Fabrication for Biochemical Sensing: Towards Point-of-Care Diagnostics. *J. Mater. Chem. B* **2021**, *9* (40), 8378−8388.

(6) Li, C.; Huang, Y.; Li, X.; Zhang, Y.; Chen, Q.; Ye, Z.; Alqarni, Z.; Bell, S. E. J.; Xu, Y. Towards Practical and Sustainable SERS: A Review of Recent Developments in the Construction of Multifunctional Enhancing Substrates. *J. Mater. Chem. C Mater.* **2021**, *9* (35), 11517−11552.

(7) Le Ru, E. C.; Etchegoing, P. *Principles of Surface Enhanced Raman Spectroscopy and Related Plasmonic Effects*; Elsevier: Amsterdam, 2009; pp 1−28.

(8) Bell, S. E. J.; Charron, G.; Cortés, E.; Kneipp, J.; de la Chapelle, M. L.; Langer, J.; Procházka, M.; Tran, V.; Schlücker, S. Towards Reliable and Quantitative Surface-Enhanced Raman Scattering (SERS): From Key Parameters to Good Analytical Practice. *Angew.Chem. Int. Ed* **2020**, *59* (14), 5454−5462.

(9) Heeg, S.; Mueller, N. S.; Wasserroth, S.; Kusch, P.; Reich, S. Experimental Tests of Surface-enhanced Raman Scattering: Moving beyond the Electromagnetic Enhancement Theory. *J. Raman Spectrosc.* **2021**, *52* (2), 310−322.

(10) Lipovka, A.; Fatkullin, M.; Averkiev, A.; Pavlova, M.; Adiraju, A.; Weheabby, S.; Al-Hamry, A.; Kanoun, O.; Pašti, I.; Lazarevic-Pasti, T.; Rodriguez, R. D.; Sheremet, E. Surface-Enhanced Raman Spectroscopy and Electrochemistry: The Ultimate Chemical Sensing and Manipulation Combination. *Crit Rev. Anal Chem.* **2024**, *54* (1), 110−134.

(11) Brolo, A. G.; Fan, M. Silver Nanoparticles Self Assembly as SERS Substrates with near Single Molecule Detection Limit. *Phys. Chem. Chem. Phys.* **2009**, *11* (34), 7381−7389.

(12) Jarvis, R. M.; Johnson, H. E.; Olembe, E.; Panneerselvam, A.; Malik, M. A.; Afzaal, M.; O'Brien, P.; Goodacre, R. Towards Quantitatively Reproducible Substrates for SERS. *Analyst* **2008**, *133* (10), 1449−1452.

(13) Santos, J. J.; Toma, S. H.; Corio, P.; Araki, K. Key Role of Surface Concentration on Reproducibility and Optimization of SERS Sensitivity. *J. Raman Spectrosc.* **2017**, *48* (9), 1190−1195.

(14) Yavuz, E.; Sakir, M.; Onses, M. S.; Salem, S.; Yilmaz, E. Advancements in Reusable SERS Substrates for Trace Analysis Applications. *Talanta* **2024**, *279*, No. 126640.

(15) Malik, U.; Hubesch, R.; Koley, P.; Mazur, M.; Mehla, S.; Butti, S. K.; Brandt, M.; Selvakannan, P. R.; Bhargava, S. Surface Functionalized 3D Printed Metal Structures as next Generation Recyclable SERS Substrates. *Chem. Commun.* **2023**, *59* (90), 13406−13420.

(16) Wu, J.; Du, Y.; Wang, C.; Bai, S.; Zhang, T.; Chen, T.; Hu, A. Reusable and Long-Life 3D Ag Nanoparticles Coated Si Nanowire Array as Sensitive SERS Substrate. *Appl. Surf. Sci.* **2019**, *494*, 583−590.

(17) Chi, H.; Wang, C.; Wang, Z.; Zhu, H.; Mesias, V. St. D.; Dai, X.; Chen, Q.; Liu, W.; Huang, J. Highly Reusable Nanoporous Silver Sheet for Sensitive SERS Detection of Pesticides. *Analyst* **2020**, *15*, 5158−5165.

(18) Li, Y.; Zhao, H.; Raza, A.; Clemmen, S.; Baets, R. Surface-Enhanced Raman Spectroscopy Based on Plasmonic Slot Waveguides with Free-Space Oblique Illumination. *IEEE J. Quantum Electron.* **2020**, *56* (1), 1−8.

(19) Li, S.; Xia, L.; Yang, Z.; Zhou, M.; Zhao, B.; Li, W. Hybrid Plasmonic Grating Slot Waveguide with High Field Enhancement for an On-Chip Surface-Enhanced Raman Scattering Sensor. *Appl. Opt.* **2020**, *59* (3), 748.

(20) Michon, J.; Kita, D.; Hu, J. Sensitivity Comparison of Free-Space and Waveguide Raman for Bulk Sensing. *J. Opt Soc. of America B* **2020**, *37*, 2012−2020.

(21) Bär, J.; De Barros, A.; De Camargo, D. H. S.; Pereira, M. P.; Merces, L.; Shimizu, F. M.; Sigoli, F. A.; Bufon, C. C. B.; Mazali, I. O. Silicon Microchannel-Driven Raman Scattering Enhancement to Improve Gold Nanorod Functions as a SERS Substrate toward Single-Molecule Detection. *ACS Appl. Mater. Interfaces* **2021**, *13* (30), 36482−36491.

(22) Bär, J.; de Barros, A.; Shimizu, F. M.; Sigoli, F. A.; Bufon, C. C. B.; Mazali, I. O. Synergy of Shaped-Induced Enhanced Raman Scattering to Improve Surface-Enhanced Raman Scattering Signal in the Thiram Molecule Detection. *Spectrochim Acta A Mol. Biomol Spectrosc* **2024**, *310*, No. 123907.

(23) Mamichev, D. A.; Timoshenko, V. Y.; Zoteyev, A. V.; Golovan, L. A.; Krutkova, E. Y.; Laktyunkin, A. V.; Kashkarov, P. K.; Astrova, E.

V.; Perova, T. S. Enhanced Raman Scattering in Grooved Silicon Matrix. *Phys. Status Solidi B Basic Res.* **2009**, *246* (1), 173−176.
(24) de Barros, A.; Shimizu, F. M.; de Oliveira, C. S.; Sigoli, F. A.; dos Santos, D. P.; Mazali, I. O. Dynamic Behavior of Surface-Enhanced Raman Spectra for Rhodamine 6G Interacting with Gold Nanorods: Implication for Analyses under Wet versus Dry Conditions. *ACS Appl. Nano Mater.* **2020**, *3* (8), 8138−8147.
(25) Paulovich, F. V.; Moraes, M. L.; Maki, R. M.; Ferreira, M.; Oliveira, O. N., Jr.; de Oliveira, M. C. F. Information Visualization Techniques for Sensing and Biosensing. *Analyst* **2011**, *136* (7), 1344.
(26) Neto, M. P.; Paulovich, F. V. Explainable Matrix - Visualization for Global and Local Interpretability of Random Forest Classification Ensembles. *IEEE Trans Vis Comput. Graph* **2021**, *27* (2), 1427−1437.
(27) Neto, M. P.; Soares, A. C.; Oliveira, O. N.; Paulovich, F. V. Machine Learning Used to Create a Multidimensional Calibration Space for Sensing and Biosensing Data. *Bull. Chem. Soc. Jpn.* **2021**, *94* (5), 1553−1562.
(28) Scarabelli, L.; Sánchez-Iglesias, A.; Pérez-Juste, J.; Liz-Marzán, L. M. A "Tips and Tricks" Practical Guide to the Synthesis of Gold Nanorods. *J. Phys. Chem. Lett.* **2015**, *6* (21), 4270−4279.
(29) Bond, A. D. Polymorphism in Molecular Crystals. *Curr. Opin Solid State Mater. Sci.* **2009**, *13* (3−4), 91−97.
(30) Chen, J.; Wang, J.; Ulrich, J.; Yin, Q.; Xue, L. Effect of Solvent on the Crystal Structure and Habit of Hydrocortisone. *Cryst. Growth Des* **2008**, *8* (5), 1490−1494.
(31) McArdle, P.; Erxleben, A. Crystal Growth and Morphology Control of Needle-Shaped Organic Crystals. *CrystEngComm* **2024**, *26* (4), 416−430.
(32) He, H.; Wan, Y.; Li, F.; Li, T.; Ren, B. Exploring the Solvent Effect on Crystal Morphology of Naphazoline Hydrochloride: Molecular Dynamic Simulations and Experiments. *J. Mol. Liq.* **2024**, *397*, No. 123908.
(33) Costa, J. C. S.; Ando, R. A.; Camargo, P. H. C.; Corio, P. Understanding the Effect of Adsorption Geometry over Substrate Selectivity in the Surface-Enhanced Raman Scattering Spectra of Simazine and Atrazine. *J. Phys. Chem. C* **2011**, *115* (10), 4184−4190.
(34) Rubira, R. J. G.; Camacho, S. A.; Aoki, P. H. B.; Maximino, M. D.; Alessio, P.; Martin, C. S.; Oliveira, O. N.; Fatore, F. M.; Paulovich, F. V.; Constantino, C. J. L. Detection of Trace Levels of Atrazine Using Surface-Enhanced Raman Scattering and Information Visualization. *Colloid Polym. Sci.* **2014**, *292* (11), 2811−2820.
(35) Eskandari, V.; Kordzadeh, A.; Zeinalizad, L.; Sahbafar, H.; Aghanouri, H.; Hadi, A.; Ghaderi, S. Detection of Molecular Vibrations of Atrazine by Accumulation of Silver Nanoparticles on Flexible Glass Fiber as a Surface-Enhanced Raman Plasmonic Nanosensor. *Opt Mater. (Amst)* **2022**, *128*, No. 112310.
(36) Albarghouthi, N.; MacMillan, P.; Brosseau, C. L. Optimization of Gold Nanorod Arrays for Surface Enhanced Raman Spectroscopy (SERS) Detection of Atrazine. *Analyst* **2021**, *146* (6), 2037−2047.

https://doi.org/10.1021/acsanm.4c07289
ACS Appl. Nano Mater. 2025, 8, 10287−10296